01 Jan 1972

Dissolution Potentials And Activation Energies Of InSb Single Crystals

Martin E. Straumanis
Missouri University of Science and Technology

Lih da Hu

Recommended Citation

M. E. Straumanis and L. d. Hu, "Dissolution Potentials And Activation Energies Of InSb Single Crystals," *Journal of the Electrochemical Society*, vol. 119, no. 7, pp. 818 - 822, The Electrochemical Society, Jan 1972.
The definitive version is available at https://doi.org/10.1149/1.2404347

Dissolution Potentials and Activation Energies of InSb Single Crystals

Dissolution Potentials and Activation Energies of InSb Single Crystals

M. E. Straumanis* and Lih-da Hu

Departments of Metallurgical and Chemical Engineering and Graduate Center for Materials Research, University of Missouri-Rolla, Rolla, Missouri 65401

ABSTRACT

The rest (or corrosion) and dissolution potentials of InSb single crystals in HCl were determined. There is no potential difference (within error limits) between the inverse {111} faces in pure HCl. A difference of up to 44 mV and more develops as soon as the InSb electrode is anodically dissolved. The potential becomes less noble in the sequence In{111}, {100}, {110}, Sb{$\bar{1}\bar{1}\bar{1}$}. The Tafel relationship is observed over three decades of current density. With additions of $FeCl_3$, $FeCl_2$, $K_3Fe(CN)_6$, $K_4Fe(CN)_6$, $H_2C_4H_4O_6$ to 2*N* HCl, the anodic potentials of both inverse {111} faces are shifted to more active values; the ϵ'_H of In{111} is always nobler than that of Sb{$\bar{1}\bar{1}\bar{1}$}. There are indications that the various potentials observed are a function of current density within the pores of a protective layer, $Sb_4O_5Cl_2$. The apparent activation energy, *ca.* 20 kcal/mole, of the anodic dissolution reaction is nearly the same on all crystallographic planes of InSb. The rate of anodic dissolution of Sb{111} in pure 2*N* HCl is 3-7 times larger than that of the inverse face at the same potential.

In a previous publication (1) the anodic dissolution reaction of InSb single crystals in HCl was described and the cited literature can be found there. However, no potential measurements were made. The anodic potentials obtained for a InSb single crystal electrode under various conditions of corrosion or dissolution are reported here.

The construction of the electrode and the type of contact with the crystal were similar to that of GaAs (2); the potentials were measured against a normal calomel electrode using a salt bridge (~3.5*N* KCl) and a Luggin capillary. The data were reduced to the standard hydrogen scale. The measurements were performed with a precision potentiometer and the potential (ϵ')-current density, *i*, curves were obtained by potentiostatic and galvanostatic methods. Purified N_2 was introduced into the reaction vessel containing the electrodes.

The n-type, undoped single crystals were obtained from the Monsanto Company (St. Louis, Missouri) and were grown in the [111] direction by the Czochralski or the gradient-freeze technique. The impurity level was less than 1 ppm, the carrier concentration was 8×10^{15} atoms·cm^{-3}, mobility 1.7×10^5 cm^2·V^{-1}·sec^{-1}, and the resistivity 0.005 ohm·cm; 670 etch pits·cm^{-2} were developed on the {111} planes. The surface area subjected to the electrolyte was between 0.35-0.82 cm^2 for the various electrodes.

Results

Rest potentials.—The potential readings were taken as soon as possible after the electrode was chemically pre-etched with CP-4 (1). Then the next reading was made after 5 min and subsequent readings after 15 min intervals. No anodic current was applied.

The results are summarized in Fig. 1. Figure 1 shows that:

1. The ϵ_H's of the inverse {111} faces in the same concentration of HCl are approximately equal, $\Delta\epsilon'_H \sim = 10$ mV; however In{111} has a slightly more noble potential than does Sb{111}.
2. For both inverse {111} faces, the higher the normality of HCl, the less noble is the ϵ'_H.
3. Time has no particular influence on ϵ'_H; steady potentials are usually obtained after 15 min of immersion.
4. The potentials are reproducible within ±10 mV.

Significant potential changes occurred in the presence of Fe^{3+}, added as $FeCl_3$ to the HCl. The potentials of the inverse {111} faces differed by as much as ~40 mV; the In{111} faces were always more positive than the Sb{$\bar{1}\bar{1}\bar{1}$}. However, the behavior of the InSb electrode in the presence of Fe^{3+} employing no anodic current required further investigation.

Anodic potential-current density relationship in 2N HCl.—The anodic potential measurements were carried out as previously described (1, 2). The platinized platinum electrode serving as the cathode was coupled with the InSb electrode. During each run, the time, milliammeter and potentiometer readings were recorded. The readings were taken after 5 min at each milliammeter setting. All current densities were plotted against the measured anodic potential (SHE). The oxygen was excluded (N_2 atmosphere).

The separation of the dissolution potentials into those characteristic of the In{111} and Sb{$\bar{1}\bar{1}\bar{1}$} faces occurred even at low anodic current densities. The potentials were in the vicinity of those of InSb in 2*N* HCl as shown in Fig 1. At a current density of 3×10^{-3} mA/cm^2 the difference was about 12 mV. This increased with increasing current density (Fig. 2). It is evident from Fig. 2 that:

1. The ϵ'_H of the four different faces becomes less noble in the sequence: In{111}, {100}, {110}, Sb{$\bar{1}\bar{1}\bar{1}$}.

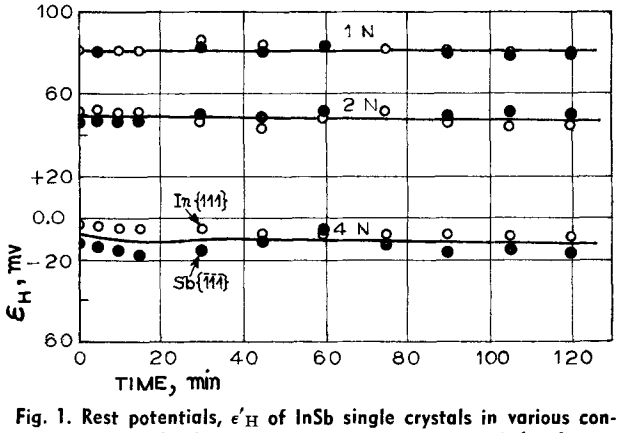

Fig. 1. Rest potentials, ϵ'_H of InSb single crystals in various concentrations of HCl (reagent grade) at 25°C. ○–In{111} and ●–Sb{111} faces.

*Electrochemical Society Active Member.

Key words: InSb, dissolution potentials, activation energies, Tafel lines.

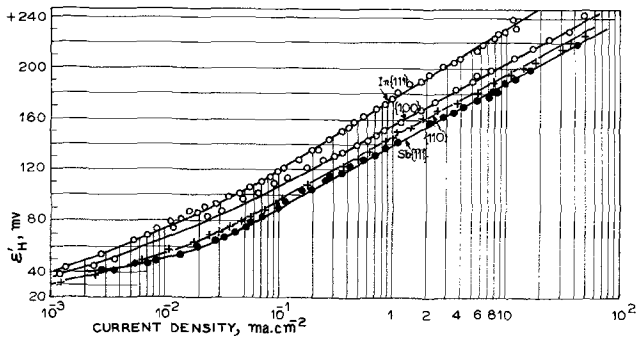

Fig. 2. Anodic dissolution potentials ϵ'_H of InSb vs. log of current density i of the single crystal planes In{111}, Sb{$\bar{1}\bar{1}\bar{1}$}, {110}, and {100} at 25°C. 2N HCl.

The potential difference between the inverse 111-faces approaches 30 mV at 3×10^{-2} mA/cm^2 and 44 mV at 10 mA/cm^2.

2. All four anodic polarization curves obey the Tafel relation over about three decades of current density (3×10^{-2} to 30 mA/cm^2).

3. Within this range of current density the latter three faces give parallel Tafel lines with a slope of ~48 mV/log i, while the first line has a slope of ~56 mV/log i. However, significant departures from these potentials occur upon addition of oxidizers or reducers to the HCl.

ϵ'_H-log i relationship in 2N HCl in the presence of Fe^{3+}.—The results of these measurements are summarized in Fig. 3, where the Tafel lines of InSb in pure 2N HCl are redrawn to show the influence of Fe^{3+}. The Tafel region occurs only between 1 and 10 mA/cm^2. Clearly, in the presence of Fe^{3+} ions, the potentials of both inverse {111} faces are shifted to more active values by approximately the same amount (~ 33 mV in 0.0004M and 37 mV in 0.002M solutions of Fe^{3+}). The slope of the Tafel line of In{111} in both solutions is 62 mV/log i and that of Sb{$\bar{1}\bar{1}\bar{1}$} is about 58 mV/log i.

Similar measurements were also performed by adding $FeCl_2$ solutions to the 2N HCl. As the solutions were prepared in air, part of the Fe^{2+} ions oxidized

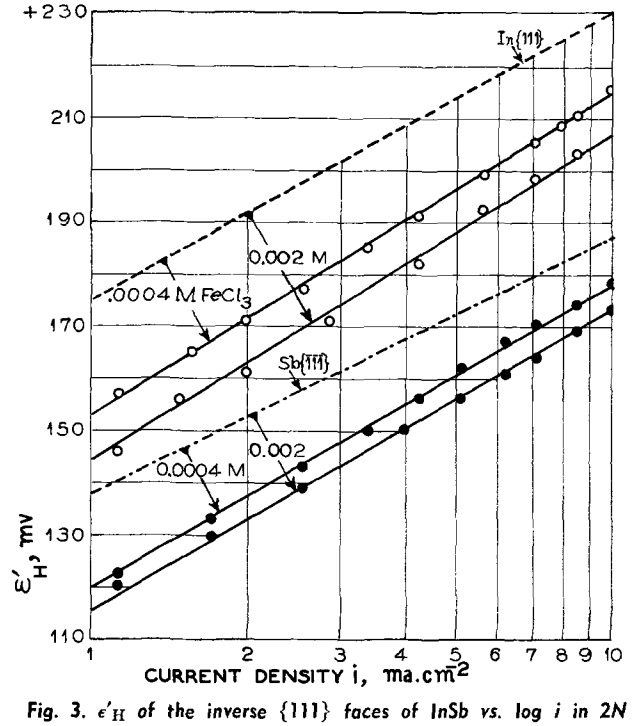

Fig. 3. ϵ'_H of the inverse {111} faces of InSb vs. log i in 2N HCl in presence of Fe^{3+} at 25°C. Dashed lines — ϵ'_H in pure 2N HCl.

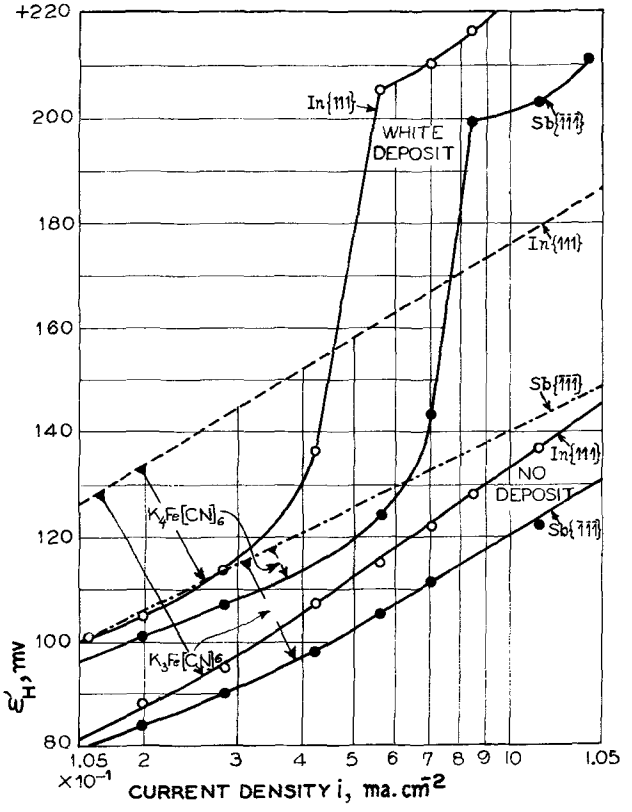

Fig. 4. ϵ'_H of the inverse {111} planes of InSb vs. log i in 2N HCl in presence of 0.00125M solutions of $K_4[Fe(CN)_6]$ and of $K_3[Fe(CN)_6]$. Dashed lines — ϵ'_H in pure 2N HCl.

to Fe^{3+} and, therefore, the results obtained resembled those with Fe^{3+}. There was a shift of potentials to more active values; however, the polarization lines were not as parallel as shown in Fig. 3.

The influence of $K_4[Fe(CN)_6]$ and of $K_3[Fe(CN)_6]$ on the anodic potential.—The ϵ'_H-log i curves in the presence of potassium ferro and ferri cyanides are shown in Fig. 4. The influence of the cyanides was observed even below 1 mA cm^{-2}. The potentials of the inverse {111} planes shifted to more active values, the action of $K_3[Fe(CN)_6]$ being stronger. No deposit was observed on the anodes when $K_3[Fe(CN)_6]$ was added. However, a white sediment appeared on both inverse faces in the presence of $K_4[Fe(CN)_6]$ at current densities above 0.4 mA/cm^2. In all the measurements the potential of the In{111} face was more positive than that of the Sb{$\bar{1}\bar{1}\bar{1}$}. Evidently the potential changes were connected with the formation and presence of deposits on the anodic surfaces. This possibility was checked by trying to remove chemically the oxide layer which is formed on Sb (of the InSb) in HNO_3.

Potentials of InSb in HNO_3 in the presence of tartaric acid.—It is known that antimony oxide dissolves in $H_2C_4H_4O_6$ yielding water-soluble, antimony-tri-tartrate. Polarization curves of the InSb{111} inverse planes are reproduced in Fig. 5. They show that, indeed, at low anodic current densities (up to 0.3 mA/cm^{-2}), the potentials of both faces coincide. A possible explanation is offered in the discussion. The Tafel relationship is nevertheless partially fulfilled.

Activation energies.—The chosen temperature of the water bath, containing the U-vessel with the InSb and Pt electrodes, was maintained at ± 0.2°C. Purified N_2 was bubbled slowly through the electrolyte (HCl). Figure 6 shows the curves obtained for the inverse {111} planes of InSb. As can be seen, the anodic dissolution potential ϵ'_H for both inverse {111} planes becomes less noble with increasing temperature and the Tafel lines exist over three decades of i. The slopes differ slightly: 55.6 mV/log i for In{111} and 47.1 for

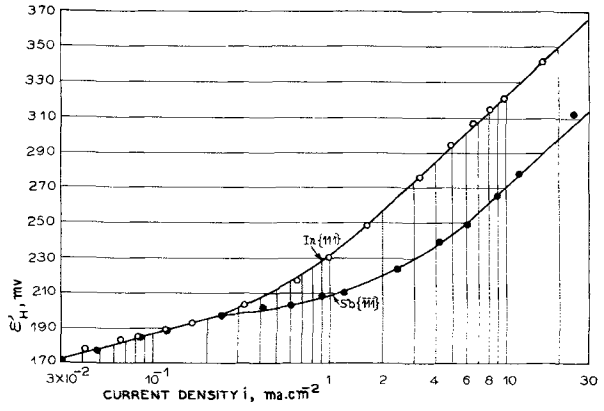

Fig. 5. ϵ'_H of the inverse {111} planes of InSb *vs.* log of anodic current density in 1*N* HNO_3-1*N* $H_2C_4H_4O_6$ at 25°C.

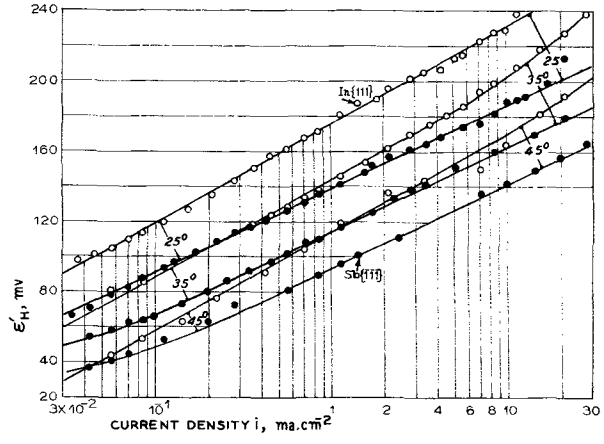

Fig. 6. ϵ'_H of In{111} and Sb{$\bar{1}\bar{1}\bar{1}$} *vs.* log *i* in 2*N* HCl at three temperatures. Galvanostatic measurements.

Sb{$\bar{1}\bar{1}\bar{1}$}. The In{111} faces are always nobler than the inverse by ~ 36, 27, and 20 mV at 25°, 35°, and 45°C respectively.

Current density measurements for four different crystal planes of InSb, were plotted against T^{-1} (Fig. 7).

The apparent activation energies E_a were calculated (Table I) from the slopes of the lines (Fig. 7).

Discussion

As InSb consists of two elements, it is interesting to see what the dissolution potentials of the latter are relative to that of InSb. In Fig. 8 the respective potentials are plotted *vs.* log *i*.

Figure 8 reveals that the dissolution potentials of the inverse {111} faces are close to that of Sb and at a current density of 1 mA/cm² there is no difference within experimental error limits. However, metallic Sb starts to passivate at about 15 mA/cm², whereas the Sb{$\bar{1}\bar{1}\bar{1}$} face remains active at higher current densities and the Tafel relationship results over nearly 3½ decades of log *i*. Evidently In, which passes simultaneously into solution (1), prevents the formation of a tight, adherent Sb-oxychloride protective layer on the InSb. In fact a thicker layer can be removed easily with a soft brush (1). Metallic In, which displays a

Table I. E_a for the anodic reactions on various planes of InSb in 2*N* HCl

Plane	E_a galvanost. kcal/mole	E_a potentiost. kcal/mole
In 111	24.0	21.3
Sb $\bar{1}\bar{1}\bar{1}$	21.3	20.1
110	—	20.3
100	—	18.5
	Average	20.05

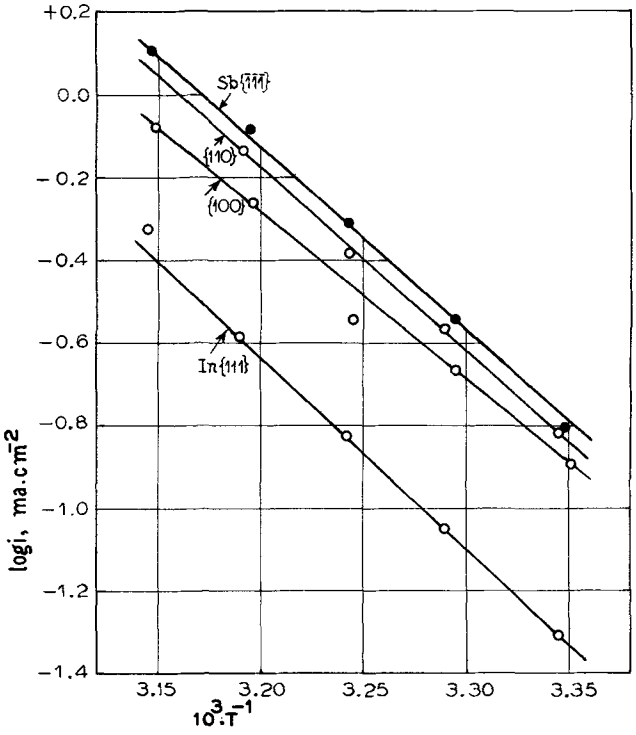

Fig. 7. Arrhenius plot of the anodic dissolution of four planes of InSb single crystals in 2*N* HCl.

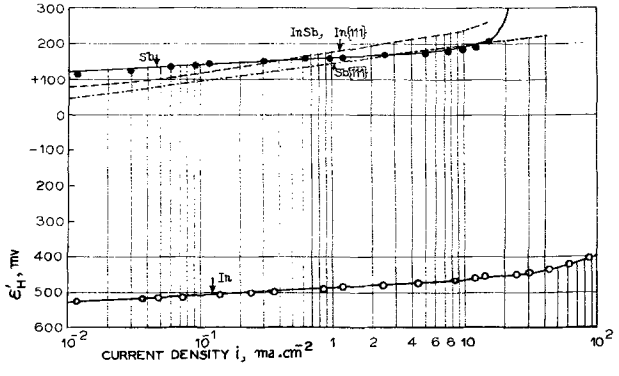

Fig. 8. ϵ'_H of metallic In, metallic Sb (both 99.999% pure) and of the inverse faces of InSb *vs.* log *i* in 2*N* HCl, 25°C.

very negative potential in 2*N* HCl (Fig. 8) loses much of its free energy by combining with Sb. Thus, the In in InSb might be in a form which is more electropositive than the Sb. At high anodic current densities part of the latter accumulates on the surface and is embedded in the oxychloride layer (anodic disintegration of Sb). This results in a lower electron number for InSb [Ref. (1), Fig. 6].

For immersion of InSb into pure 2*N* HCl, where the corrosion rate is very low [Ref. (1), Table I], the protective layers formed on all crystallographic faces are evidently of the same consistency and adherence. Therefore, there is little, if any, potential difference between the inverse {111} faces and the potential is strongly dependent on the *p*H of the solution (Fig. 1) as it is for a pure Sb electrode (3, 4).

However, as soon as an anodic current is applied, the oxychloride layer is at least partially removed from the various faces of the InSb crystal. The difference in valency of the two constituents now comes into play and this can be noticed, especially on the inverse {111} planes. The potential difference between these planes is the greatest among those investigated and the potentials become more negative in the order: In{111}, {100}, {110} and Sb{$\bar{1}\bar{1}\bar{1}$} (Fig. 2). Explanations of this difference have been offered by other authors (5, 6). GaAs in KOH behaves similarly (2) (Fig. 3).

If now at the same current density various crystallographic planes exhibit different anodic potentials (Fig. 2), it can be assumed (if InSb behaves like a metal) that this is due to the difference in the structure of the protective films. During anodic dissolution both inverse {111} planes of InSb are covered with a Sb-oxychloride film (1), but this film may be, for unknown reasons, more dense and/or more adherent to the In{111} rather than to the Sb{$\bar{1}\bar{1}\bar{1}$} plane. Moreover, it is also probable that In (within the InSb structure), due to the loss of free energy, is present in a different form, than in a metal, and now has less ability to go into solution. Both assumptions contribute to the presence of a more noble potential on the In{111} than on the Sb{$\bar{1}\bar{1}\bar{1}$} face, especially under conditions of anodic dissolution. The other planes should exhibit intermediate values. This anodic behavior, as a current density effect, requires a smaller pore size on the In{111} face which results in a higher current density within the pores and a steeper Tafel line will be obtained (Fig. 2). When the anodic current is decreased, the quality of the previous oxide film on the faces will be restored and consequently the potential difference between the inverse {111} planes will diminish (Fig. 2) and finally approach zero (Fig. 1).

Therefore, agents which partially remove the Sb-oxide film from the InSb electrode should also decrease the potential difference between the inverse planes. This is the case when InSb is dissolved in 1*N* HNO_3 containing tartaric acid (Fig. 5). At low current densities the oxide film is thin on both planes, since the newly formed Sb-oxide easily dissolves in tartaric acid. However, at current densities above 0.3 mA · cm^{-1} the thickness of the film increases so much that the dissolution of the film is not rapid enough and a separation of the potentials occurs. The film on the In{111} should be denser. This follows from the inclination of the Tafel lines: at low current densities—26 mV/log *i* and above 4 mA · cm^{-2} ~ 92 mV/log *i*. Furthermore the potential of InSb in 1*N* HNO_3 is much more positive than in HCl (compare Fig. 2 and 5) caused partially by the difference in the composition and properties of the layers. Denser oxide or hydroxide films are formed in HNO_3 because of the oxidizing action of the acid.

Increasing the concentration of a nonoxidizing acid (*e.g.*, HCl) should decrease the thickness of the surface oxide layers, which results in a more negative potential, as shown in Fig. 1.

Similar to the behavior of the Sb electrode, the potential of the InSb electrode is very easily disturbed by oxidizing and reducing agents, and it is difficult to understand this disturbance. For instance (Fig. 3), minute amounts of $FeCl_3$ added to 2*N* HCl shift the potential of both inverse {111} planes to less noble values, the shift increasing with increasing concentration of the Fe^{3+} ions. Nevertheless the Tafel line relationship persists and the In{111} planes are always nobler than the inverse. Evidently Fe^{3+} ions are adsorbed by the oxychloride layer, changing its properties, increasing its pore size, which results in a lower pore current density and in a more active potential.

The action of $K_4Fe(CN)_6$ and of $K_3Fe(CN)_6$ additions is still more complicated. In both cases the potential of the anode becomes more negative relative to the dissolution potentials in pure 2*N* HCl (see Fig. 4). Again the In{111} is more noble than the inverse face.

If the InSb is anodically dissolved in a 2*N* HCl-0.00125*M* $K_4Fe(CN)_6$ solution, then at current densities higher than 0.4 mA·cm^{-2} the formation of a white collodial layer is observed on both inverse {111} planes. The layer can be removed by rinsing with water. No deposit was observed in a 2*N* HCl-0.00125M $K_3Fe(CN)_6$ solution, even at current densities above 10 mA · cm^{-2}. According to Mellor (7) $K_4Fe(CN)_6$ forms a white precipitate with In^{3+} but $K_3Fe(CN)_6$ does not. This was confirmed experimentally. Thus the jump in the curves (Fig. 4) is explained as the onset of the precipitate formation. At about 1 mA · cm^{-2} the precipitate is already so dense that one can see it readily. Thus this surface layer causes a strong polarization, which does not occur for $K_3Fe(CN)_6$, because the salt formed is water soluble and the slope of the Tafel-lines above 0.6 mA·cm^{-2} is ~ 70 mV for In{111} and 60 mV for Sb{$\bar{1}\bar{1}\bar{1}$}.

With increasing temperature the dissolution potentials become more negative (Fig. 6) partially because of thermodynamic reasons and also due to the decrease of the anodic current density within the pores (widening of the pores with increasing temperature).

Since the slopes of the Tafel lines fluctuate mostly between 40 and 60 mV/log *i*, the possibility of a one electron charge transfer as a rate-determining step is not excluded. Nevertheless, the rate of dissolution in pure 2*N* HCl of Sb{$\bar{1}\bar{1}\bar{1}$} at the same potential is 3-7 times larger than that of the inverse face, in agreement with the concept of pore width. Evidently, the effective current density (within the pores) is the same on all the faces. However, as the pores of the protective layer on Sb{$\bar{1}\bar{1}\bar{1}$} are larger, a stronger current results from this face.

The apparent activation energies (Table I) for the anodic reactions on various planes of InSb are the same within the error limits, suggesting that the reactions (1) are all the same, independently of the plane chosen for the anode. However, the E_a value of ~ 20 kcal/mole is relatively high for a dissolution reaction. A similar value of 16.7 kcal/mole was also obtained for the anodic dissolution reaction of the compound GaAs in KOH (2). Much lower activation energies were found for metals simply dissolving in acids, *e.g.*, 5.3 ± 0.5 kcal for Hf dissolving in 1*N* HF or in a mixture of HF and HCl (8) and 3.8 to 4.2 kcal for Zr in 0.2*N* HF or 0.1*N* HF + 1.0*N* HCl respectively (9). However, when the oxygen content of Zr was increased up to 7% b.w., the E_a increased to 5.9 kcal. Simultaneously the rate of dissolution decreased, evidently the dissolved oxygen tightly bound by the Zr atoms hampered the reaction rate with the acid.

As InSb exhibited a much lower dissolution rate (1), a higher activation energy should be expected for this reaction, because it is chiefly the value of E_a which determines the rate (10), even of an anodic dissolution process. The activation energy of ~ 20 kcal/mole was, therefore, expected. Thus a high activation energy of dissolution of InSb (and of GaAs) in comparison with that of pure metals is characteristic of the former and corresponds to its reaction sluggishness.

Acknowledgments

The authors are grateful to Dr. W. J. James, Professor of Chemistry and Director of the Graduate Center for Materials Research, for assisting with the present manuscript, and to the New Enterprise Division of the Monsanto Company in St. Louis, especially to Mr. J. B. McNeely, for donation of the InSb single crystals.

This is Contribution No. 135 from the Graduate Center for Materials Research.

Manuscript submitted Nov. 11, 1971; revised manuscript received March 6, 1972.

Any discussion of this paper will appear in a Discussion Section to be published in the June 1973 JOURNAL.

REFERENCES

1. M. E. Straumanis and Lih-da-Hu, *This Journal*, **118**, 433 (1971).
2. M. E. Straumanis, J. P. Krumme, and W. J. James, *ibid.*, **115**, 1050 (1968).
3. H. T. S. Britton and R. A. Robinson, *J. Chem. Soc.*, **1931**, 458.
4. H. T. S. Britton, "Hydrogen Ions," Vol. I, Van Nostrand, Princeton (1956).
5. H. C. Gatos and M. C. Lavine, *This Journal*, **107**, 427 (1960)

6. H. C. Gatos and M. C. Lavine, *J. Phys. Chem. Solids*, **14**, 169 (1960).
7. J. W. Mellor, "A Comprehensive Treatise of Inorganic and Theoretical Chemistry" Vol. V, pp. 393-397; Vol. IX, pp. 378-388 and 503-509, Longmans, Green & Co., London (1922).
8. W. J. James, J. W. Johnson, and M. E. Straumanis, *Z. Physik. Chem.*, **27**, 199 (1961).
9. W. J. James, W. G. Custead, and M. E. Straumanis, *Corrosion Sci.*, **2**, 237 (1962).
10. A. J. Rutgers "Physical Chemistry," p. 627, Interscience Publishers, New York (1953).

The Effect of Two-Dimensional Nucleation on the Rate of Electrocrystallization

Ugo Bertocci

Solid State Division, Oak Ridge National Laboratory, Oak Ridge, Tennessee 37830

ABSTRACT

The effect of random two-dimensional nucleation on current-potential curves, valid for epitaxial electrodeposition on single-crystal faces, has been examined employing a specific model for nucleation and surface step motion. Computations have been performed for the electrodeposition of silver and copper: for the first metal the results are in reasonable agreement with some experimental data concerning two-dimensional nucleation on close-packed surfaces. In the case of copper the agreement with experimental results seems to be less satisfactory. The influence of assumptions, such as the type of surface step distribution, on the rate of electrocrystallization has been examined and discussed. Computer simulations of potentiostatic transients have also been carried out, and some effects of suppressing nucleation in the vicinity of steps have been investigated.

From computer-simulated experiments on the influence of two-dimensional nucleation and step motion on the rate of crystal growth (1), formulas have been obtained which allow one to estimate the relative importance of random nucleation and step density on the growth rate. The purpose of the present paper is to apply these results to the case of electrocrystallization processes, attempting to evaluate current-potential curves for the deposition of metals on close-packed and vicinal surfaces of single-crystal electrodes.

Models and Methods of Calculation

In the epitaxial growth of a single crystal by electrocrystallization, the current density i depends on the density and velocity of the steps moving on the surface

$$i = \frac{z\mathbf{F}h_{(hkl)}}{V_m} V\theta \qquad [1]$$

where z is the number of electrons exchanged, $h_{(hkl)}$ is the height of a crystal layer in the [hkl] direction, V_m the molar volume, and V and θ the step velocity and step density. If the dependence of the current density on the overvoltage η has to be found, it is necessary to express V and θ as a function of overvoltage. The step velocity can be considered in general to depend on η and θ and an expression will be derived later (Eq. [13]). Steps on the surface can be due to misorientation with respect to a close-packed plane (the step density due to misorientation is indicated as ζ) or to the interplay between two-dimensional nucleation rate R_n and step velocity V. The formula relating these quantities is (1)

$$\theta = \sqrt[3]{\frac{2R_n}{V} + \zeta^3} \qquad [2]$$

and our purpose is to obtain the dependence of R_n and V, and therefore θ, on the overvoltage.

According to nucleation theory (2), R_n is given by the product of the concentration of critical nuclei, which are formed by aggregating adatoms over the close-packed portions of the surface, the rate of addition of single adatoms to the critical nucleus, and the Zeldovich nonequilibrium factor

$$R_n = Z\, n_{cr}\, \omega \qquad [3]$$

Since two-dimensional nucleation is considered here, nuclei are assumed to be cylindrical in shape, their height being one atom layer. The concentration of critical nuclei is

$$n_{cr} = NA \exp\left(-\frac{\Delta G^{\ddagger} + \Delta G_q + \Delta G_s}{kT}\right) \qquad [4]$$

where N is Avogadro's number and A the concentration of unaggregated adatoms (in mol/cm^2); $\Delta G^{\ddagger}$ is the free energy for the formation of a nucleus

$$\Delta G^{\ddagger} = -\frac{\pi h_{(hkl)}\gamma^2 V_m}{\Delta\mu} \qquad [5]$$

where γ is the surface energy and $\Delta\mu$ is the decrease in free energy in the crystallization process. ΔG_q is the contribution to the free energy due to the distribution of nuclei on the various sites of the substrate. The number of such sites is equal to $Nd_{(hkl)}$ where $d_{(hkl)}$ is the surface density of the close-packed layer (hkl) (in mol/cm^2).

$$\Delta G_q = \frac{kT}{A}\left[d_{(hkl)} \ln\left(\frac{d_{(hkl)} - A}{d_{(hkl)}}\right) + A \ln\left(\frac{A}{d_{(hkl)} - A}\right)\right] \qquad [6]$$

Calling K the ratio $d_{(hkl)}/A$ where K is a constant greater than 1, Eq. [6] becomes

$$\Delta G_q = kT \ln\left[\frac{A}{d_{(hkl)}}\left(\frac{K-1}{K}\right)^{K-1}\right] \qquad [7]$$

The free energy of separation, as defined by Lothe and Pound (3), is

$$\Delta G_s = kT \ln\left(\sqrt{2\pi i_{cr}}\right) \qquad [8]$$

where i_{cr} is the number of atoms in the critical nucleus.

Key words: electrodeposition, electrochemistry, computer simulations, copper, silver.